Two-photon lifetime-based photoconversion of EGFP for 3D-photostimulation in FLIM

Methods and Applications in Fluorescence

PAPER

Two-photon lifetime-based photoconversion of EGFP for 3D-photostimulation in FLIM

Dita Strachotová[1,3], **Aleš Holoubek**[2,3], **Barbora Brodská**[2] and **Petr Heřman**[1,*]

[1] Faculty of Mathematics and Physics, Institute of Physics, Charles University, Ke Karlovu 5, 121 16 Prague 2, Czech Republic
[2] Institute of Hematology and Blood Transfusion, U Nemocnice 2094/1, 128 20 Praha 2, Czech Republic
[3] Both authors contributed equally.
[*] Author to whom any correspondence should be addressed.

E-mail: herman@karlov.mff.cuni.cz

Keywords: fluorescence lifetime imaging, photoconversion, two-photon imaging, cellular tracking, protein dynamics, nucleophosmin, histone H2B

OPEN ACCESS

RECEIVED
23 December 2022

REVISED
18 May 2023

ACCEPTED FOR PUBLICATION
1 June 2023

PUBLISHED
12 June 2023

Abstract

Enhanced green fluorescence protein (EGFP) is a fluorescent tag commonly used in cellular and biomedical applications. Surprisingly, some interesting photochemical properties of EGFP have remained unexplored. Here we report on two-photon-induced photoconversion of EGFP, which can be permanently converted by intense IR irradiation to a form with a short fluorescence lifetime and spectrally conserved emission. Photoconverted EGFP thus can be distinguished from the unconverted tag by the time-resolved detection. Nonlinear dependence of the two-photon photoconversion efficiency on the light intensity allows for an accurate 3D localization of the photoconverted volume within cellular structures, which is especially useful for kinetic FLIM applications. For illustration, we used the two photon photoconversion of EGFP for measurements of redistribution kinetics of nucleophosmin and histone H2B in nuclei of live cells. Measurements revealed high mobility of fluorescently tagged histone H2B in the nucleoplasm and their redistribution between spatially separated nucleoli.

Abbreviations

EGFP_NPM	nucleophosmin tagged by EGFP
FLIM	fluorescence lifetime imaging
FP	fluorescent protein
FRAP	fluorescence recovery after photobleaching
NPM	nucleophosmin
TPE	two-photon excitation
TPPc	two-photon-induced photoconversion
TPPc-EGFP	EGFP photoconverted using two-photon absorption
TPPc-EGFP_NPM	nucleophosmin tagged by TPPc-EGFP
wtGFP	wild-type GFP

1. Introduction

Fluorescent proteins (FPs) are widely used for imaging of dynamic cellular processes, monitoring of gene expression, protein tracking, and localization [1, 2]. FPs frequently exhibit complex photochemical behavior. Emission properties of a number of them can be light-shifted between various emitting states [3–5]. Photoactivatable fluorescent proteins can be photoconverted from dark to bright emitting state, photoswitchable FPs permanently shift from one fluorescent state to another, and reversibly switchable FPs can be repeatedly light-toggled between spectrally distinct fluorescent states by proper illumination [5]. New photo-manipulable variants of FPs have often opened new application fields ranging from cellular protein tracking and rapid cellular dynamics to multicolor and superresolution imaging [5–7].

Fast proliferation of FP mutants and their applications often cause a lag between their usage and thorough physical and photochemical characterization [8].

For this reason, users of such molecules should rather cautiously interpret their data. Sometimes even notoriously known FPs like EGFP can reveal overlooked properties that, unrecognized, can seriously bias experimental data. It could be e.g. unwanted spectral photoconversion during photobleaching known as redding [9, 10], greening [11], or lifetime-based photoconversion [12]. However, with proper knowledge, these drawbacks can be turned to advantages in new applications [12].

EGFP is an extensively used fluorescent tag. It exhibits good quantum yield, large extinction coefficient and absorption and emission compatible with common excitation sources and microscopes, efficient folding, low oligomerization, and high photostability [13, 14]. EGFP can be also efficiently excited by the two-photon excitation (TPE) with the cross section σ_2 close to 40 GM [15]. All these features are desirable for quantitative microscopy. Over the years, EGFP has been well characterized [e.g. 13, 16–22] and validated for use in the cell research [12, 23]. The tag is widely spread, easily available, and remains the green FP of choice for many researchers [24]. Recently we have revealed that EGFP can be permanently photoconverted to a form with a shorter fluorescence lifetime. While under gentle illumination EGFP has been found fairly photostable and resistant to photodestruction [1, 25, 26], strong blue illumination to the first singlet absorption band causes a lasting reduction of its excited state lifetime without noticeable spectral shifts [12]. Though there are number of FPs photoconvertible between spectrally distinct forms [2, 27, 28], the emission rates can be light-manipulated only for a few of them. In addition to EGFP, this property has also been reported for ECFP and Cerulean [29]. This group of lifetime-convertible FPs is extremely desirable and useful for fluorescence lifetime imaging (FLIM) [30].

Compared to the conventional single-photon-excited laser scanning FLIM, its two-photon variant exhibits a number of advantages in biomedical and cellular research [31–33]. A quadratic dependence of the two-photon absorption rate on the light intensity causes excitation only at the focal point where the photon flux is large enough to induce fluorescence [34]. This implies an inherent sectioning capability permitting elimination of the photon-wasting confocal pinhole in the detection light path and improved photon efficiency [33]. Since the absorption occurs only at the small femtoliter-sized volume, the overall photodamage of the sample is reduced, which is highly desirable in experiments requiring prolonged sample illumination [15]. Infrared excitation better penetrates the scattering samples and allows for deep tissue imaging [35, 36]. Due to the antistokes emission, scattering and autofluorescence of the sample can be efficiently suppressed.

An intriguing task of cellular biophysics is an evaluation of the diffusion and redistribution of macromolecules in live cells [37], especially between tiny cellular compartments [38, 39]. A conical single-photon excitation beam results in a photodamage, photoactivation or photoconversion along the whole excitation light path and subsequent loss of the ability to accurately 3D-position the photoconverted volume. Importantly, due to the nonlinear intensity dependence, the two-photon excited or photoconverted spot can be well localized within the 3D sample and allows for more accurate targeting of the subcellular structures. Two-photon-induced photoconversion (TPPc) is therefore well suited for the investigation of 3D-diffusion and transport processes on the subcellular scale [32]. Unlike FRAP, TPPc does not require complete photodestruction of fluorophores in the activated area. As a consequence, mixing of signals from the unconverted and photoconverted protein can be followed in time.

Here we present a two-photon photoconversion of EGFP resulting in a fluorescent EGFP form with reduced fluorescence lifetime and spectrally conserved emission. The photoconverted protein is easily separable from the unconverted form by lifetime imaging and serves as a suitable light-inducible lifetime highlighter for FLIM. We show that unlike the single-photon conversion, the strong dependence of the two-photon photoconversion on the light intensity allows for accurate 3D localization of the photoconverted volume within the cell. This is especially useful for kinetic FLIM applications, e.g. for exploration of cellular diffusion, protein redistribution, etc [40]. Importantly, only a single spectral channel is needed for the detection while the other ones stay free for multispectral imaging. Moreover, the inherently ratiometric nature of emission lifetimes allows for elimination of artifacts commonly accompanying any intensity-based measurements. As an application example of the TPPc-FLIM technique, we present visualization of the redistribution of EGFP-tagged nucleophosmin (EGFP_NPM) between nucleoli of live HEK-293T cells. The second application example shows TPPc-FLIM measurement of redistribution kinetics of EGFP-labeled histone H2B (EGFP_H2B) in the nucleus of live HeLa cells, which documents diffusive communication between separated nucleoli and rapid exchange of H2B between them.

2. Materials and methods

2.1. Cell cultivation and transfections

Adherent HEK-293T and HeLa cells were cultured at 37 °C under standard cultivation conditions in DMEM (Gibco) or RPMI (Sigma), respectively. The cell cultures were supplemented with 10% FBS (Biochrom) and 5% CO_2 atmosphere. Live-cell experiments were performed at 37 °C after sealing the glass-bottomed Petri dish (Cellvis) with parafilm to prevent CO_2 leakage. Plasmids coding for free EGFP

(peGFP-C2, Clontech), EGFP_NPM (NPM subcloned to peGFP-C2) [41], and EGFP_H2B (Addgene plasmid #11680; http://n2t.net/addgene:11680; RRID: Addgene_11680 [42], a gift from G. Wahl) were handled as described elsewhere [12].

Specifically, the plasmids were amplified in *E. coli* and purified with PureYield Plasmid Miniprep System (Promega). The cells were seeded to 1.5×10^5 ml^{-1} cell density, incubated for 24 h and transfected using jetPrime transfection reagent (Polyplus Transfection) according to the manufacturer's protocol. The transfected cells were further grown for 20–40 h prior to experiment.

2.2. Cell fixation

EGFP-producing cells grown on a glass-bottom Petri dish were fixed with 4% paraformaldehyde and permeabilized by 0.5% Triton X-100 as described earlier [12]. The permeabilization was used merely for compatibility with the original protocol that ensures faster equilibration of the fixed cells. Finally, the cells were submerged in the sterile PBS and stored in 4 °C. Experiments with fixed cells were done at room temperature.

2.3. Fluorescence lifetime imaging

FLIM measurements were performed on the apparatus described in detail elsewhere [12]. Briefly, we used an inverted IX83 microscope equipped with a FV1200 confocal scanner (Olympus, Hamburg, Germany), a cultivation chamber, and FLIM add-ons from PicoQuant (Berlin, Germany). Single photon emission was excited by the LDH-DC-485 pulsed laser emitting at 482 nm with 20 MHz repetition rate (PicoQuant, Berlin, Germany). Laser output coupled to the microscope by a single-mode optical fiber was reflected to the sample by the 488 nm long-pass dichroic mirror (Olympus). Emission was collected through the 520/34 bandpass filter (Semrock, New York, USA).

Two-photon imaging was done on the same microscope using a free-space-coupled IR beam from the Ti:Saphire laser (Chameleon Ultra2, Coherent, Santa Clara, California) running at 80 MHz. The group-delay dispersion was pre-compensated by a pulse compressor (Thorlabs, Dachau, Germany) and the IR light was reflected to the sample by the RDM 690 dichroic mirror (Olympus). Depending on the experiment, fluorescence was directed to the cooled GaAsP hybrid PMTs (PicoQuant) either through a liquid light guide mounted on the non-descanned port or via a multimode optical fiber mounted on the descanned port. EGFP fluorescence was spectrally isolated using the 520/34 bandpass filter (Semrock) and the residual IR excitation was blocked by the 680/SP filter (Semrock). Time-resolved data were acquired by the TimeHarp 260-PICO TCSPC card and processed by the SymPhoTime64 software (PicoQuant). To minimize pile-up artifacts [43], the data collection rate for the brightest pixels was kept below 5% of the excitation frequency. Typically, we used UPLSAPO60XW water immersion objective (NA 1.2) or UPLSAPO30XS silicone oil immersion objective (NA 1.05) (Olympus). Experiments with fixed and live cells were done at 25 °C and 37 °C, respectively.

For the rapid FLIM imaging, the end of photoconversion was synchronized with the start of the FLIM acquisition. A series of several hundreds of FLIM images was immediately collected with the FLIM frame rate of 2 frames/s. The obtained multiframe FLIM stack allowed for construction of the lifetime evolution in any selected ROI of the image.

2.4. Two-photon photoconversion

Photoconversion was performed by scanning a selected ROI with live monitoring of the emission intensity. Depending on the excitation wavelength, type of the experiment and a particular sample, the mean power of the IR laser was set between 10–40 mW at the focal point of the objective. Typically, we finished the photoconversion when the emission intensity of EGFP decreased to about 20%–30% of its initial value. For time-undemanding experiments the TPPc was done gradually with standard scanning and lower light power within 2–4 min. For the rapid FLIM experiments the photoconverted area and the photoconversion light intensity was adjusted to complete TPPc within few seconds using the 'turbo bleach' mode of the microscope.

2.5. Data processing

As described earlier [12], FLIM images were constructed by the 'fast-FLIM' approach using the SymPhoTime64 software. Briefly, pixel lifetimes were determined by the method of moments [44] when τ_{avg} is a difference between the barycentre of the emission decay and the time-offset of the steepest growth of the decay, t_{offset}:

$$\tau_{avg} = \sum_i I_i t_i \Big/ \sum_i I_i - t_{offset} \qquad (1)$$

where I_i stands for the decay intensity at time t_i. FLIM data were further processed and visualized in the Fiji software [45]. More accurate analyses of the cumulative decays from larger ROIs were done by the least-squares reconvolution. Fluorescence was assumed to decay multiexponentially according to the formula:

$$I(t) = \sum_i \alpha_i \cdot \exp(-t/\tau_i), \ \sum_i \alpha_i = 1 \qquad (2)$$

where τ_i and α_i are the fluorescence lifetime components and corresponding amplitudes, respectively. Typically, two decay components were sufficient for acceptable fits with χ^2 below 1.3. The intensity-weighted mean fluorescence lifetime was calculated as:

$$\tau_{mean} = \sum_i f_i \tau_i = \sum_i \alpha_i \tau_i^2 \Big/ \sum_i \alpha_i \tau_i \qquad (3)$$

where f_i are the fractional intensities of the i-th lifetime component:

$$f_i = \alpha_i \tau_i / \sum_i \alpha_i \tau_i, \ \sum_i f_i = 1 \quad (4)$$

The deconvolution was performed either using the SymphoTime or the FluoFit software (PicoQuant, Berlin, Germany). Both packages allow for the so-called 'cyclic excitation correction', which corrects for the incomplete emission decay between two successive excitation pulses [46, 47]. We used the correction for the deconvolution of TPE decays excited at 80MHz when excitation pulse separation of ~12.5 ns did not allow for a sufficient decay of EGFP with ~2.5 ns lifetime. As a result, unbiased fluorescence lifetimes were extracted from the incomplete decays collected with high repetition rate excitation, which is typical for the two-photon imaging.

3. Results

EGFP undergoes photoconversion to a spectrally indistinguishable form with shorter fluorescence lifetime upon intense illumination to the first singlet absorption band [12]. Here we tested whether the similar effect can be achieved with the two-photon excitation and utilize its better 3D-localization for kinetic and protein-tracking experiments using two-photon fluorescence microscopy.

Figure 1 demonstrates the TPPc experiment on HEK-293T cells producing free EGFP. To prevent EGFP diffusive mixing of the photoconverted and unconverted molecules, we fixed the sample by paraformaldehyde, which immobilized the fluorophore and allowed for better visualization of the photoconverted volume. TPE fluorescence intensity and FLIM images are presented in the first and the second column, respectively. The first row shows the sample before the TPPc. From the intensity images we clearly recognize cytoplasm and nuclei of the stained cells. As expected, the mean EGFP fluorescence lifetime τ_{mean} = 2.52 ns is mostly homogeneous across the cells both in the XY- and XZ-planes (panel B and H, respectively). Then the area marked by the white rectangle was scanned by strong 920 nm light. In order to increase illuminated volume in the Z-direction, five confocal scans with the focal plane shifted by 0.2 μm in the Z-direction were sequentially performed. The process was repeated until fluorescence from the irradiated area decreased to about 30% of the initial value, panel C. The TPE-FLIM image acquired immediately after the photoconversion is shown in figure 1(D). We can clearly distinguish the photoconverted area in the lifetime image where τ_{mean} of EGFP decreased from 2.52 ns to 2.32 ns upon the irradiation. Confocal X-Z sections corresponding to panels A-D are shown in panels G-J. The position of the X-Z section is marked by the red line. We can see spatially well-localized volume of photoconverted EGFP. To evaluate reversibility of TPPc, the sample was stored at dark in 4 °C and reimaged 24 h later. Figures 1(E), (F) document that the photoconverted area is still distinguishable with only insignificant drift in lifetimes. The corresponding X-Z sections are shown in figures 1(K), (L). Intensity and lifetime profiles across the photoconverted nucleus before and after TPPc are presented in figures 1(M), (N). The drop in the lifetime profile is clearly visible and correlates with change of the intensity profile. Figure 2 shows differences between the spatial localization of the single- and two-photon photoconversion performed side-by-side on two nucleoli of a fixed cell with EGFP-tagged nucleolar protein nucleophosmin. Compared to figure 1, we aimed at much smaller objects, since nucleoli are sub-nuclear structures. The X-Z FLIM-sections of the nucleoli reveal that the focused single- and two-photon light-beams targeted into the nucleoli make different imprints in the Z-direction of the originally uniform lifetime distribution. As seen from the lifetime profiles in figure 2(E), the single-photon process induces photoconversion that extends almost across the whole nucleolus (FWHM 3.4 μm) compared to the better axially localized TPPc (FWHM 1.6 μm). This TPPc property allows for photoconversion of smaller volumes and targeting smaller cellular structures.

Further we investigated the two-photon excitation efficiency of the photoconverted EGFP for different excitation wavelengths. Figure 3 shows TPE confocal images of the fixed sample where EGFP in the right cell was subjected to TPPc (white rectangle). The left cell served as a control. Visual inspection of panels A and B reveals stronger TPE emission of TPPc-EGFP when it is excited by 1050 nm compared to the 850 nm excitation. Intensity profiles across the converted and control cells shown in figure 3(C) document that the two-photon excitation efficiency of TPPc-EGFP increases at longer excitation wavelength. This is further supported by the ratio of emission intensities of the photoconverted and unconverted EGFP ($I_{TPPc\text{-}EGFP}/I_{EGFP}$) shown in figure 3(D) and overlaid with the two-photon absorption spectrum of EGFP [15]. The $I_{TPPc\text{-}EGFP}/I_{EGFP}$ ratio exhibits a minimum close to the two-photon absorption peak of EGFP and increases toward longer wavelengths. Data indicate that the TPE spectrum of TPPc-EGFP is likely red-shifted compared to the one of the unconverted protein.

3.1. Exchange of NPM between nuclear structures

We examined suitability of TPPc for investigation of diffusive kinetic processes in live cells. Nucleophosmin (NPM) is an abundantly expressed multifunctional nucleolar phosphoprotein participating e.g. in cellular stress response via complex interaction network [48]. In healthy cells NPM exhibits nucleolar localization [49, 50], which may be altered by drugs or pathogenic mutations [51, 52]. Diverse NPM roles and cellular interactions require free trafficking of NPM in the nucleus and cytoplasm. Nevertheless, not much is known about NPM mobility and dynamics [53, 54]. Figure 4 shows typical redistribution of EGFP_NPM

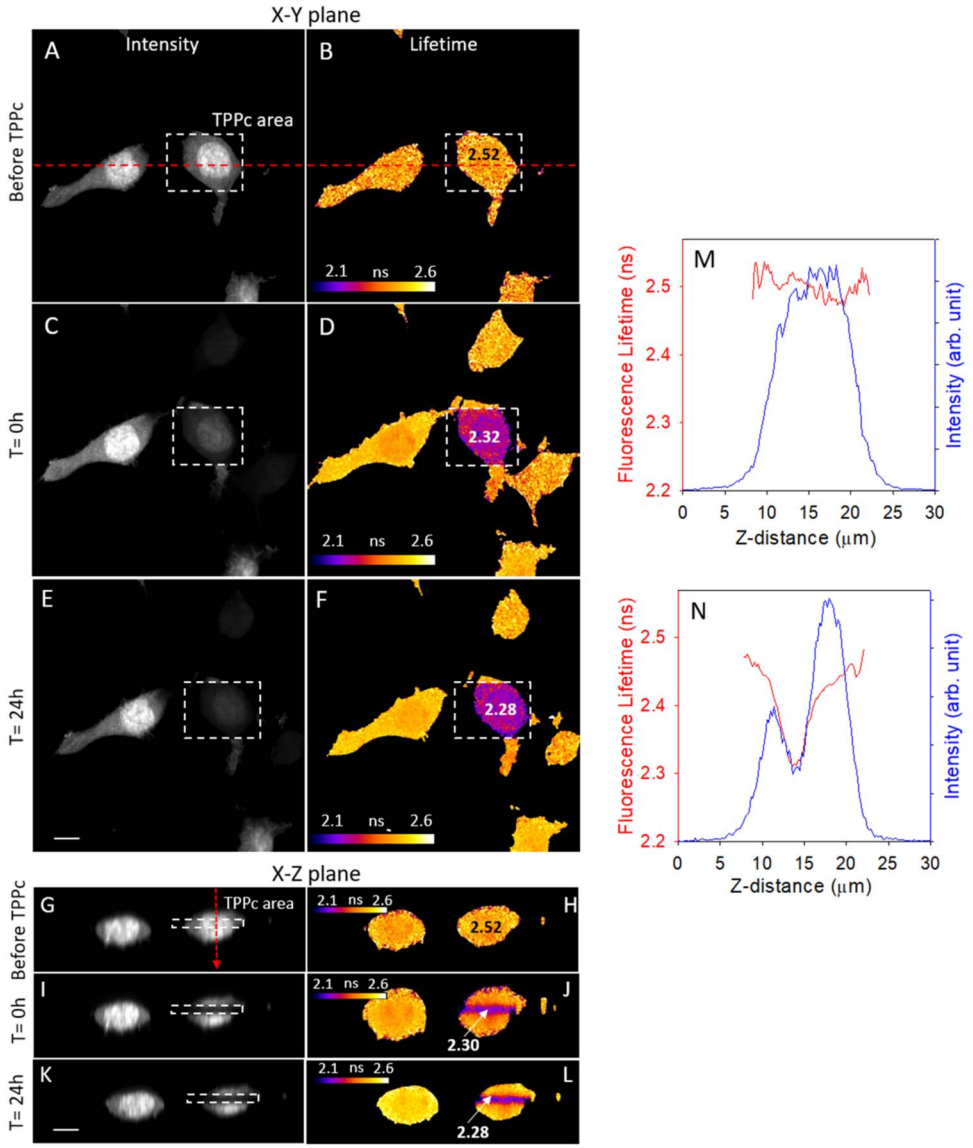

Figure 1. Two-photon-induced photoconversion of EGFP. Two-photon intensity and FLIM images (the 1st and the 2nd column, respectively) of free EGFP in fixed HEK-293T cells before TPPc (A), (B), (G), (H), just after TPPc (T = 0h, (C), (D), (I), (J) and 24 h later (T = 24h, (E), (F), (K), (L). Panels A-F represent scans in the X-Y image plane, panels G-L are perpendicular X-Z sections. Position of the X-Z section is indicated by the red line in (A), (B). The photoconverted area is marked by the white rectangle. TPPc was performed by 920 nm light in 5 focal planes shifted by 0.2 μm in the axial Z-direction (the white rectangle in (G), (I), (K). Then the sample was kept for 24h at 4 °C and re-imaged. (M), (N) - Fluorescence intensity and lifetime profiles in the Z-direction before (M) and after (N) TPPc. The direction of the profiles is marked by the red arrow in (G). Bar 10 μm, TPPc laser power 15 mW at the focal point of the UPLSAPO30XS objective.

in live HEK-293T cell upon perturbation of its equilibrium by localized TPPc. The shorter τ_{mean} of TPPc-EGFP allows its tracking by FLIM. Figures 4(A), (B) show the equilibrium intensity and FLIM images of EGFP_NPM before photoconversion. As expected, EGFP_NPM is localized preferentially in spatially separated nucleoli, the NPM level in the nucleoplasm outside nucleoli is dramatically lower, and fluorescence from the cytoplasm is undetectable, figure 4(A). For the convenience, the nuclear area of one cell is marked by the yellow dashed line. The FLIM image in figure 4(B) reveals τ_{mean} being 2.26 ns in the nucleoli. The slight lifetime difference between the nucleoli and the nucleoplasm results from different local environments of EGFP [55], e.g. from the different local refraction index [12, 56, 57]. The localized TPPc was done by a brief illumination of a small nucleolar volume by intense IR light and after few minutes the sample was reimaged, figures 4(D)–(F). From the FLIM image we can see that TPPc-EGFP_NPM with shorter τ_{mean} spreads from the illuminated spot over the whole nucleus and appears in all spatially separated nucleoli of the photoconverted cell. The separation can be seen from the X-Z section images shown in figures 4(G), (I). TPPc-FLIM data suggest rapid exchange of TPPc-EGFP_NPM among all nucleoli of the treated cell, as documented by the decreased τ_{mean} in the whole volume of the untreated nucleoli caused by mixing of the converted and unconverted protein.

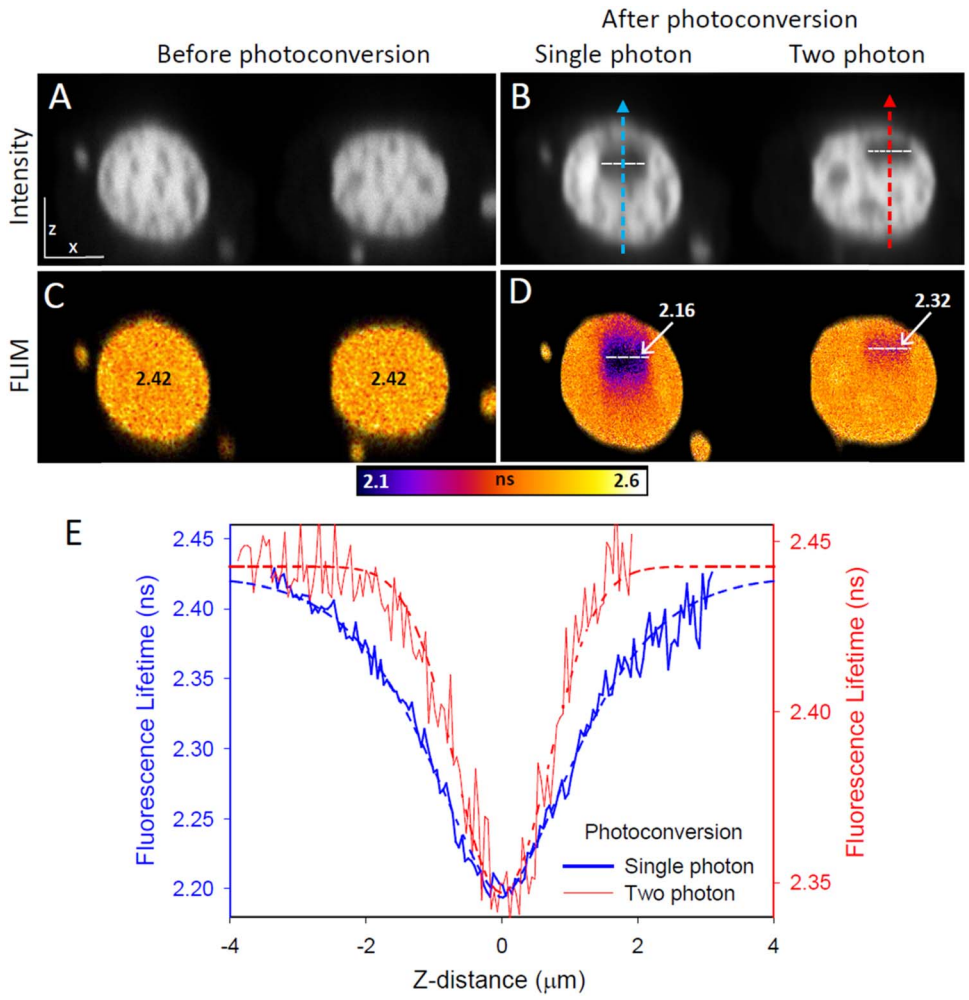

Figure 2. Comparison of the spatial localization of single- and two-photon photoconversion in fixed HEK-293T cell. X-Z-section of two adjacent nucleoli in a cell containing EGFP_NPM. (A) and (C)—intensity and FLIM image of the nucleoli before photoconversion, respectively. (B) and (D)—the nucleoli after the photoconversion. Photoconversion was performed in a single focal plane by 488 nm and 870 nm light in the left and right nucleolus, respectively. The X-Z projection of the photoconverted circular ROI is marked by the dashed line in (B), (D). (E) - Fluorescence lifetime profiles across the nucleoli after the photoconversion. The direction of the profiles is marked by arrows in (B). Bar—3 μm, UPLSAPO60XW objective, single photon imaging with 488 nm excitation.

All NPM redistribution was completed within minutes.

3.2. Rapid nuclear dynamics of histone H2B

Nucleosomes are dynamic structures carrying diverse regulatory functions including gene expression, epigenetic silencing, packaging and condensing the genome, see e.g. [58, 59] for review. Histone H2B is a part of this disk-shaped structure formed by the hetero-octameric complex assembled from two H2A-H2B and H3-H4 histone hetero dimers wrapped by 146 base pairs of DNA [60]. Due to the tight association of histone H2B/H2A with chromatin-bound nucleosomes, their mobility is reduced and their redistribution kinetics can be followed by time-lapse FLIM experiments.

Figure 5 presents rapid TPPc-induced redistribution kinetics of EGFP-labeled H2B (EGFP_H2B) in the nucleus of a single live HeLa cell. In the intensity image we can see the nucleus with several nucleoli accumulating EGFP_H2B, which exhibit uniform emission lifetime in all nucleoli. The fractional volume positioned at the equatorial plane of the largest nucleolus was briefly photoconverted by 870 nm light and a multi-frame series of FLIM images synchronized with the photoconversion pulse was immediately acquired. From figure 5(C) we can notice time-dependent mixing of the converted and unconverted fractions of EGFP_H2B in the illuminated nucleolus. The equilibration of the photoconverted protein between different nucleoli is visually less prominent, nevertheless, as documented in figure 5(D), it is measurable and significant. Figure 5(D) presents time-evolution of the τ_{mean} in the photoconverted focal plane of the light-treated and control nucleoli. The time-dependent lifetimes in the photoconverted nucleolus were fitted by the biexponential rising model, which revealed two characteristic redistribution times of 6 s and 150 s. The fast rising component documents rapid initial mixing of the converted and unconverted

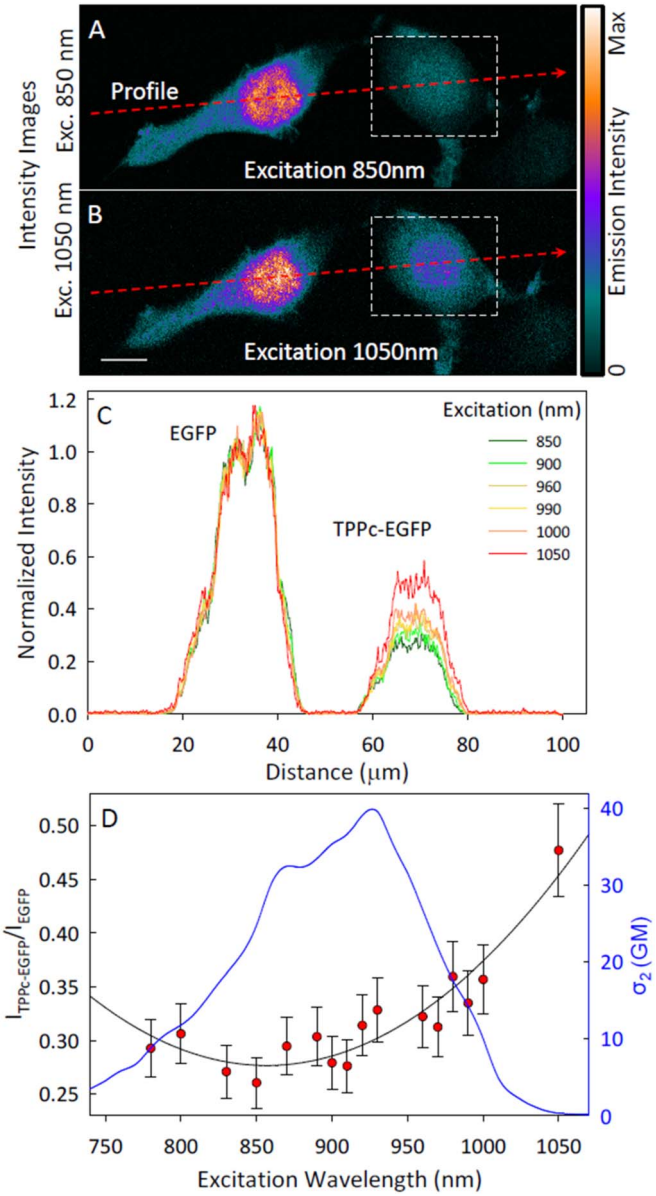

Figure 3. Two-photon excitation efficiency of TPPC-EGFP in in fixed HEK-293T cells. (A) and (B) - Two-photon fluorescence intensity images of free EGFP excited at 850 nm and 1050 nm, respectively. The area photoconverted by 920 nm light is bordered by the white rectangle. The unconverted control cell is in the left. Intensities of panels A and B were normalized at the nucleus of the control cell. (C) - Fluorescence intensity profiles for different excitation wavelengths. The direction of the profile is marked by the red arrow in panels A, B. The profiles were peak-normalized at the emission maximum of the control cell. (D) - Relative two-photon excitation efficiency of the TPPc-EGFP and EGFP (red circles) overlaid with the two-photon absorption spectrum of EGFP shown by the blue line [15]. The photoconversion and imaging conditions were the same as in figure 1, bar 10 μm.

proteins, which can be associated mainly with the redistribution of the mobile fraction of TPPc-EGFP_H2B within the photoconverted nucleolus. The longer component reflects slower processes likely associated with a dynamic exchange of bound photoconverted histones for the unconverted ones. As already mentioned, the control nucleolus also exhibits photoconversion-induced change in the mean EGFP lifetime, which speaks for free diffusion of TPPc-EGFP_H2B all around the nucleus resulting in a gradual enrichment of other nucleoli for the photoconverted protein and decreased τ_{mean}. Fitting the data in the control nucleus by the biexponential model revealed characteristic exchange times of about 5 s and 250–500 s. Interestingly, the fast mixing time closely resembles the 6s rising component in the photoconverted nucleolus and the long components are also reasonably comparable. The result suggests that a significant fraction of the tagged H2B is highly mobile. Besides the internal nucleolar mixing, TPPc-EGFP_H2B escaping from the photoconverted nucleolus very rapidly diffuses through the nucleoplasm being almost instantly trapped in other nucleoli where it equilibrates. The bi-phasic equilibration kinetics in the control and photoconverted nucleolus seem to mimic, within the experimental uncertainty, each other, which is consistent with a significant fraction of highly mobile H2B in the nucleus.

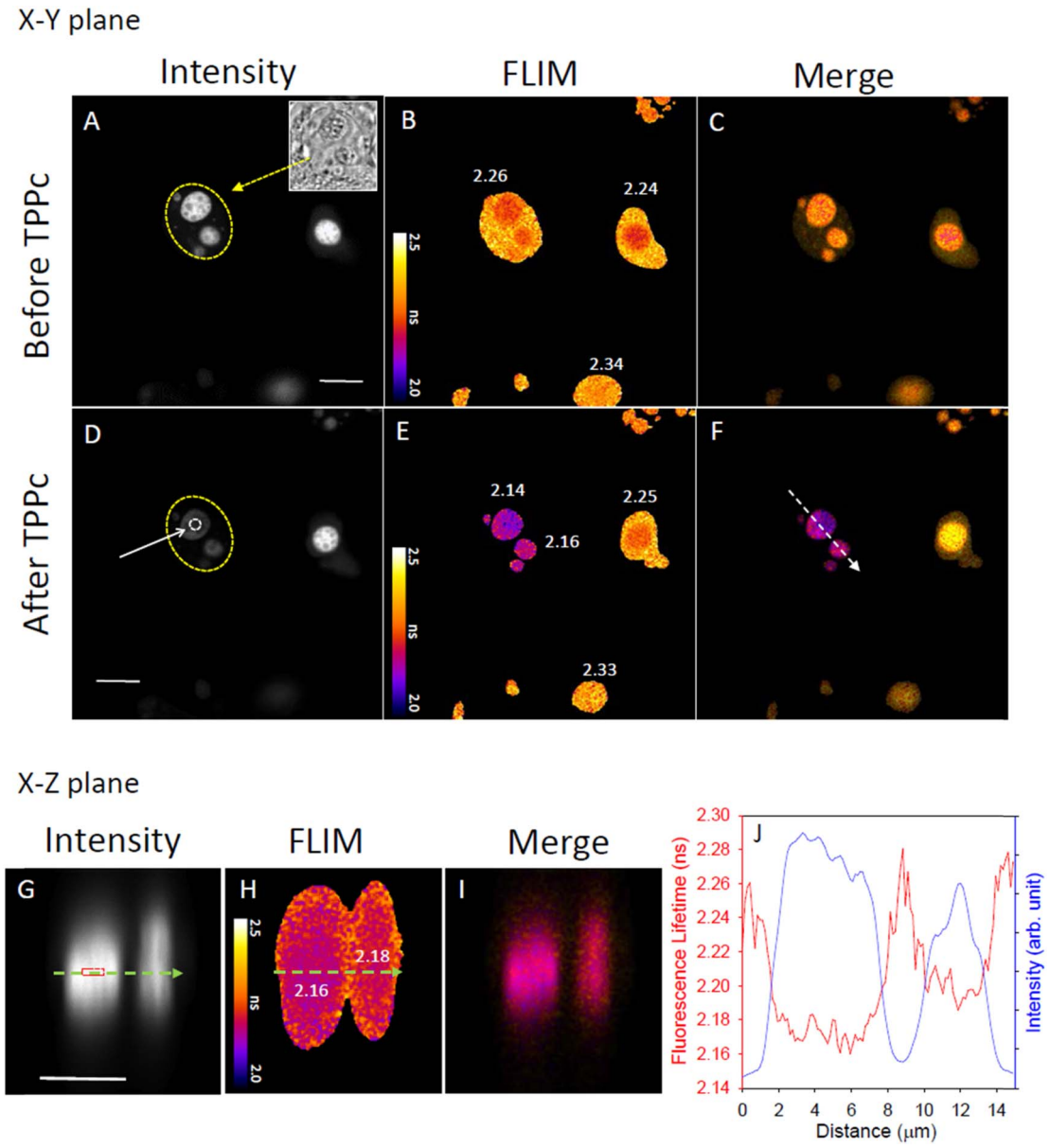

Figure 4. Distribution of EGFP_NPM in the nucleus of the live HEK-293T cell upon localized TPPc. Equilibrium intensity (A, D), FLIM (B, E) and the merged images (C), (F) before (A), (B), (C) and after (D), (E), (F) TPPc localized to the center of the nucleolus. The nucleus of interest is bordered by the yellow dashed line, the X-Y projection of the photoconverted spot is indicated by the white circle (in D), and the transmission image of the corresponding area is shown in the inset in A. (G)–(I)—Equilibrium distribution of TPPc-EGFP_NPM in the X-Z plane of the photoconverted nucleus few minutes after TPPc. The orientation of the plane is indicated by the white arrow in panel F. (G) - Intensity image. Two spatially separated nucleoli are visible, the X-Z projection of the photoconverted area is marked by the red rectangle. (H) - FLIM image, (I)—merged images (G) and (H). (J) - The intensity (blue line) and the fluorescence lifetime profile (red line) along the green arrow in (G), (H). TPPc was done by a brief illumination of the ROI by 870 nm light using UPLSAPO30XS objective and laser power of 15 mW in the focal point of the objective. Imaging was performed with the single-photon 488 nm excitation. Bar 10 μm. Representative results are presented (n = 6).

4. Discussion

A strong blue illumination photoconverts EGFP to a form with shorter fluorescence lifetime [12]. It can be therefore used as an optically activable highlighter in kinetic FLIM applications. Since the single-photon photoconversion does not exhibit any distinct intensity threshold, the overall light dosage seems to determine the photoconversion efficiency. As a consequence, the photoconverted volume in the axial Z-direction of the microscopic sample is poorly defined. It spans essentially the whole sample thickness, even though, due to the focusing the efficiency of the conversion is not uniform throughout the sample. This limitation prevents accurate 3D positioning of the photoconverted volume within the sample, which is critical for accurate targeting of small cellular compartments in tracking applications [12, 25, 63]. For instance, targeting of the interior of nucleoli, whose dimensions typically do not exceed 2 μm in live cells, is hardly possible with the single-photon excitation, as seen from figure 2(E). Here we have shown that

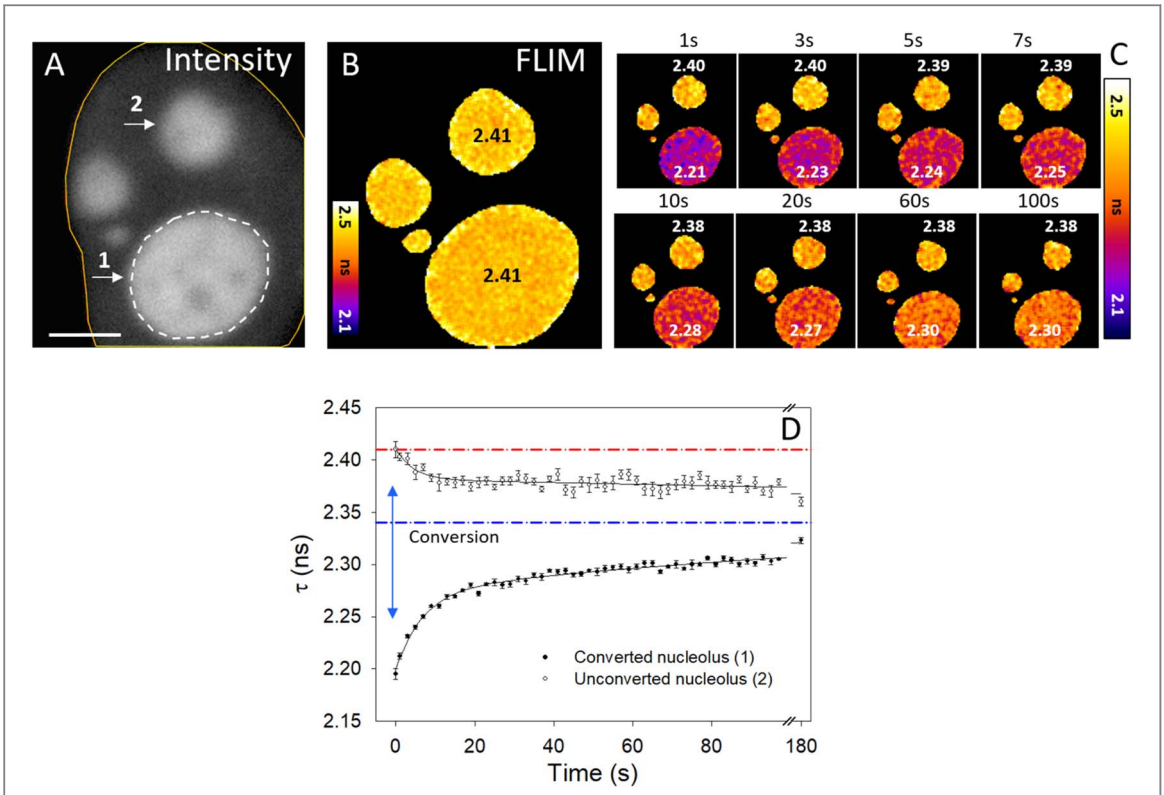

Figure 5. TPPc-induced redistribution of EGFP-labeled histone H2B in the nucleus of a single live HeLa cell. (A) - Fluorescence intensity image before TPPc (gamma = 0.7 was applied to the whole image in order to visualize the nucleoplasm).The nuclear area is bordered by the yellow line. The photoconverted (1) and the control nucleolus (2) are marked by arrows. (B) - FLIM image before TPPc, (C) - Evolution of the initial FLIM image shown in (B) upon TPPc. The photoconversion was performed in the equatorial plane of the nucleolus by 870 nm light (~35 mW in the focal plane for ~3 s). The photoconverted area is marked by the dashed line. Images were collected in the TPE nondescanned mode with 870 nm excitation and the UPLSAPO60XW water immersion objective. (D) - Detailed time-evolution of the mean fluorescence lifetime assessed by the least-squares deconvolution analysis of the signal integrated over the photoconverted and the control nucleolus. The red line corresponds to the initial lifetime, the blue line is a fit-estimated lifetime plateau in the photoconverted nucleolus. Error bars result from the bootstrap statistical analysis [61, 62] of the fluorescence decays at each particular time after the TPPc. Bar is 2 μm.

EGFP can be permanently photoconverted to the short-lived form also by the two-photon absorption process. Since this effect is nonlinear and it is supposed to depend at least quadratically on the illumination intensity, the photoconverted volume is better defined and considerably shrinks in the axial Z-direction. Consequently, it can be better localized in the examined structures, as shown in figure 2. When the TPPc is followed by the time-lapse lifetime-based imaging, it can reveal kinetic properties of both converted and unconverted proteins by simultaneous visualization of their diffusion. Since both the converted and unconverted proteins are fluorescent, mixing of their signal can be followed in time by FLIM. Such prolonged time-lapse FLIM experiments can therefore reveal also the rate of the freshly synthesized FPs, which might negatively affect standard FRAP experiments [24]. Unrecognized lifetime-based photoconversion in the vicinity of the photobleached volume, which is inevitably accompanied by changes in fluorescence intensity, may also bias quantitative analysis of both single- and two-photon FRAP with EGFP. Our approach offers milder FLIM-based alternative to the two-photon FRAP, which usually requires complete photodestruction of the fluorophore in the range of interest [36]. Importantly, TPPc is fully compatible with the two-photon imaging with all its advantages, e.g. deep imaging of thick scattering samples or elimination of artefacts rising from difference in the objective's focal length for IR photoconversion and following single photon imaging [37, 64]. Unlike intensity-based FRAP, the lifetime-based FLIM is internally ratiometric and does not suffer by common artifacts associated with intensity measurements [30].

Nuclear proteins are known to be highly mobile [65]. Histones are expected to be an exception, because they bind to the chromatin as constituents of nucleoplasm-localized nucleosomes [66]. Nevertheless, consistently with literature, we found ectopically expressed EGFP_H2B histone accumulated in nucleoli [67], since their binding sites on the chromatin are occupied by the endogenous protein with a slow exchange rate. In the nucleolus, EGFP_H2B appears to be retained by entropic forces and nonspecific electrostatic interactions with

charged nucleolar components. Our TPPc-induced EGFP_H2B redistribution measurements revealed highly mobile nucleolar fraction of EGFP_H2B with characteristic exchange time of 6 s, and a slower fraction with characteristic time of ~150 s. Results qualitatively agree well with literature FRAP data where slow and fast fractions were also identified [67]. While the whole nucleolus was bleached in the FRAP experiments, we photoconverted only an equatorial layer of the nucleolus. The TPPc-FLIM data therefore reflect not only the exchange of H2B between the nucleolus and nucleoplasm but also the 3D diffusion inside the nucleolus. Newly we also documented fast exchange of EGFP_H2B between nucleoli. The almost instant appearance of TPPc-EGFP_H2B in the unconverted nucleoli suggest very high mobility of EGFP_H2B in the nucleoplasm where the protein rapidly scans the whole nucleus until it is trapped by the proper target.

In conclusion, we have revealed permanent lifetime-based photoconversion of EGFP induced by a two-photon absorption process. Besides potential FLIM artifacts, which can be caused by an unintentional photoconversion, controlled application of TPPc turns EGFP to a valuable tool for kinetic measurements. In combination with FLIM it offers higher information content compared to FRAP. Applicability of TPPc was demonstrated on measurements of a nuclear diffusion of NPM and histone H2B, which revealed high mobility of these fluorescently tagged proteins in the nucleoplasm.

Acknowledgments

This work was supported by the Czech Science Foundation (grant No 22–03875S), and the Center of Nano- and Bio-Photonics UNCE/SCI/010.

Data availability statement

The data that support the findings of this study are available upon reasonable request from the authors.

Author contributions

PH, AH and BB designed the research; DS, AH, BB, PH performed the research; DS, PH analyzed the data; PH wrote the paper. All authors edited and commented on the manuscript.

Conflict of interest

The authors declare no conflicts of interests.

ORCID iDs

Barbora Brodská https://orcid.org/0000-0002-3703-594X
Petr Heřman https://orcid.org/0000-0001-6918-2576

References

[1] Chudakov D M, Matz M V, Lukyanov S and Lukyanov K A 2010 Fluorescent proteins and their applications in imaging living cells and tissues *Physiol. Rev.* **90** 1103–63
[2] Nienhaus K and Nienhaus G U 2014 Fluorescent proteins for live-cell imaging with super-resolution *Chem. Soc. Rev.* **43** 1088–106
[3] Acharya A, Bogdanov A M, Grigorenko B L, Bravaya K B, Nemukhin A V, Lukyanov K A and Krylov A I 2017 Photoinduced chemistry in fluorescent proteins: curse or blessing? *Chem. Rev.* **117** 758–95
[4] Bogdanov A M, Mishin A S, Yampolsky I V, Belousov V V, Chudakov D M, Subach F V, Verkhusha V V, Lukyanov S and Lukyanov K A 2009 Green fluorescent proteins are light-induced electron donors *Nat. Chem. Biol.* **5** 459–61
[5] Shcherbakova D M, Sengupta P, Lippincott-Schwartz J and Verkhusha V V 2014 Photocontrollable fluorescent proteins for superresolution imaging *Annu. Rev. Biophys.* **43** 303–29
[6] Zhou X X and Lin M Z 2013 Photoswitchable fluorescent proteins: ten years of colorful chemistry and exciting applications *Curr. Opin. Chem. Biol.* **17** 682–90
[7] Bourgeois D and Adam V 2012 Reversible photoswitching in fluorescent proteins: a mechanistic view *Iubmb Life* **64** 482–91
[8] Ward W W 2006 Biochemical and physical properties of green fluorescent protein *Properties, Applications, and Protocols, 2nd Edition* ed M Chalfie and S R Kain (Hoboken: Wiley-Interscience) pp 39–65
[9] Saha R, Verma P K, Rakshit S, Saha S, Mayor S and Pal S K 2013 Light driven ultrafast electron transfer in oxidative redding of Green Fluorescent Proteins *Sci. Rep.* **3** 1580
[10] Gorbachev D A, Petrusevich E F, Kabylda A M, Maksimov E G, Lukyanov K A, Bogdanov A M, Baranov M S, Bochenkova A V and Mishin A S 2020 A general mechanism of green-to-red photoconversions of GFP *Frontiers in Molecular Biosciences* **7** 176
[11] Kremers G J, Hazelwood K L, Murphy C S, Davidson M W and Piston D W 2009 Photoconversion in orange and red fluorescent proteins *Nat. Methods* **6** 355–8
[12] Herman P, Holoubek A and Brodska B 2019 Lifetime-based photoconversion of EGFP as a tool for FLIM *Biochimica Et Biophysica Acta-General Subjects* **1863** 266–77
[13] Tsien R Y 1998 The green fluorescent protein *Annu. Rev. Biochem.* **67** 509–44
[14] Sarkisyan K S *et al* 2015 Green fluorescent protein with anionic tryptophan-based chromophore and long fluorescence lifetime *Biophys. J.* **109** 380–9
[15] Drobizhev M, Makarov N S, Tillo S E, Hughes T E and Rebane A 2011 Two-photon absorption properties of fluorescent proteins *Nat. Methods* **8** 393–9
[16] Arpino J A J, Rizkallah P J and Jones D D 2012 Crystal structure of enhanced green fluorescent protein to 1.35 angstrom resolution reveals alternative conformations for Glu222 *PLoS One* **7** e47132
[17] Cinelli R A G, Ferrari A, Pellegrini V, Tyagi M, Giacca M and Beltram F 2000 The enhanced green fluorescent protein as a tool for the analysis of protein dynamics and localization: Local fluorescence study at the single-molecule level *Photochem. Photobiol.* **71** 771–6
[18] Cotlet M *et al* 2001 Excited-state dynamics in the enhanced green fluorescent protein mutant probed by picosecond time-resolved single photon counting spectroscopy *J. Phys. Chem.* **105** 4999–5006

[19] Haupts U, Maiti S, Schwille P and Webb W W 1998 Dynamics of fluorescence fluctuations in green fluorescent protein observed by fluorescence correlation spectroscopy *PNAS* **95** 13573–8
[20] Jimenez-Banzo A, Nonell S, Hofkens J and Flors C 2008 Singlet oxygen photosensitization by EGFP and its chromophore HBDI *Biophys. J.* **94** 168–72
[21] Royant A and Noirclerc-Savoye M 2011 Stabilizing role of glutamic acid 222 in the structure of enhanced green fluorescent protein *J. Struct. Biol.* **174** 385–90
[22] Stepanenko O V, Verkhusha V V, Kazakov V I, Shavlovsky M M, Kuznetsova I M, Uversky V N and Turoverov K K 2004 Comparative studies on the structure and stability of fluorescent proteins EGFP, zFP506, mRFP1, 'dimer2', and DsRed1 *Biochemistry* **43** 14913–23
[23] Rodriguez E A, Campbell R E, Lin J Y, Lin M Z, Miyawaki A, Palmer A E, Shu X K, Zhang J and Tsien R Y 2017 The growing and glowing toolbox of fluorescent and photoactive proteins *Trends Biochem. Sci* **42** 111–29
[24] Shaner N C, Patterson G H and Davidson M W 2007 Advances in fluorescent protein technology *J. Cell Sci.* **120** 4247–60
[25] Lippincott-Schwartz J, Snapp E and Kenworthy A 2001 Studying protein dynamics in living cells *Nat. Rev. Mol. Cell Biol.* **2** 444–56
[26] Patterson G H, Knobel S M, Sharif W D, Kain S R and Piston D W 1997 Use of the green fluorescent protein and its mutants in quantitative fluorescence microscopy *Biophys. J.* **73** 2782–90
[27] Subach O M, Patterson G H, Ting L M, Wang Y R, Condeelis J S and Verkhusha V V 2011 A photoswitchable orange-to-far-red fluorescent protein, PSmOrange *Nat. Methods* **8** 771–7
[28] Shcherbakova D M and Verkhusha V V 2014 Chromophore chemistry of fluorescent proteins controlled by light *Curr. Opin. Chem. Biol.* **20** 60–8
[29] Hoffmann B, Zimmer T, Klocker N, Kelbauskas L, Konig K, Benndorf K and Biskup C 2008 Prolonged irradiation of enhanced cyan fluorescent protein or Cerulean can invalidate Forster resonance energy transfer measurements *J. Biomed. Opt.* **13** 031205
[30] Herman P and Lakowicz J R 2014 Lifetime-based imaging *Biomedical Photonics Handbook Fundamentals, Devices, and Techniques* ed T Vo-Dingh (New York: CRC Press) 2nd edn pp 353–96
[31] Ranawat H, Pal S and Mazumder N 2019 Recent trends in two-photon auto-fluorescence lifetime imaging (2P-FLIM) and its biomedical applications *Biomed Eng Lett* **9** 293–310
[32] Rubart M 2004 Two-photon microscopy of cells and tissue *Circ. Res.* **95** 1154–66
[33] Zipfel W R, Williams R M and Webb W W 2003 Nonlinear magic: multiphoton microscopy in the biosciences *Nat. Biotechnol.* **21** 1368–76
[34] Brown E B, Shear J B, Adams S R, Tsien R Y and Webb W W 1999 Photolysis of caged calcium in femtoliter volumes using two-photon excitation *Biophys. J.* **76** 489–99
[35] Yang W J and Yuste R 2017 *In vivo* imaging of neural activity *Nat. Methods* **14** 349–59
[36] Mostany R, Miquelajauregui A, Shtrahman M and Portera-Cailliau C 2015 Two-photon excitation microscopy and its applications in neuroscience *Methods Mol. Biol.* **1251** 25–42
[37] Calvert P D, Peet J A, Bragin A, Schiesser W E and Pugh E N 2007 Fluorescence relaxation in 3D from diffraction-limited sources of PAGFP or sinks of EGFP created by multiphoton photoconversion *J. Microsc.* **225** 49–71
[38] Wei X, Henke V G, Strubing C, Brown E B and Clapham D E 2003 Real-time imaging of nuclear permeation by EGFP in single intact cells *Biophys. J.* **84** 1317–27
[39] Peet J A, Bragin A, Calvert P D, Nikonov S S, Mani S, Zhao X, Besharse J C, Pierce E A, Knox B E and Pugh E N Jr 2004 Quantification of the cytoplasmic spaces of living cells with EGFP reveals arrestin-EGFP to be in disequilibrium in dark adapted rod photoreceptors *J. Cell Sci.* **117** 3049–59
[40] Pantazis P and Supatto W 2014 Advances in whole-embryo imaging: a quantitative transition is underway *Nat. Rev. Mol. Cell Biol.* **15** 327–39
[41] Brodska B, Holoubek A, Otevrelova P and Kuzelova K 2016 Low-dose actinomycin-D induces redistribution of wild-type and mutated nucleophosmin followed by cell death in leukemic cells *J. Cell. Biochem.* **117** 1319–29
[42] Kanda T, Sullivan K F and Wahl G M 1998 Histone-GFP fusion protein enables sensitive analysis of chromosome dynamics in living mammalian cells *Curr Biol* **8** 377–85
[43] O'Connor D V and Philips D 1984 *Time-Correlated Single Photon Counting* (London: Academic)
[44] Patting M 2008 Evaluation of time-resolved fluorescence data: typical methods and problems ed U Resch-Genger *Standardization and Quality Assurance in Fluorescence Measurements I: Techniques* (Berlin, Heidelberg: Springer Berlin Heidelberg) pp 233–58
[45] Schindelin J *et al* 2012 An open-source platform for biological-image analysis *Nat Meth* **9** 676–82
[46] Sakai Y and Hirayama S 1988 A fast deconvolution method to analyze fluorescence decays when the excitation pulse repetition period is less than the decay times *J. Lumin.* **39** 145–51
[47] Walther K A, Papke B, Sinn M B, Michel K and Kinkhabwala A 2011 Precise measurement of protein interacting fractions with fluorescence lifetime imaging microscopy *Mol. Biosyst.* **7** 322–36
[48] Colombo E, Alcalay M and Pelicci P G 2011 Nucleophosmin and its complex network: a possible therapeutic target in hematological diseases *Oncogene* **30** 2595–609
[49] Sasinkova M, Herman P, Holoubek A, Strachotova D, Otevrelova P, Grebenova D, Kuzelova K and Brodska B 2021 NSC348884 cytotoxicity is not mediated by inhibition of nucleophosmin oligomerization *Sci. Rep.* **11** 1084
[50] Holoubek A, Herman P, Sykora J, Brodska B, Humpolickova J, Kracmarova M, Gaskova D, Hof M and Kuzelova K 2018 Monitoring of nucleophosmin oligomerization in live cells *Methods. Appl. Fluoresc.* **6** 035016
[51] Holoubek A, Strachotova D, Otevrelova P, Roselova P, Herman P and Brodska B 2021 AML-related NPM mutations drive p53 delocalization into the cytoplasm with possible impact on p53-dependent stress response *Cancers (Basel)* **13** 3266
[52] Brodska B, Kracmarova M, Holoubek A and Kuzelova K 2017 Localization of AML-related nucleophosmin mutant depends on its subtype and is highly affected by its interaction with wild-type NPM *PLoS One* **12** e0175175
[53] Negi S S and Olson M O 2006 Effects of interphase and mitotic phosphorylation on the mobility and location of nucleolar protein B23 *J. Cell Sci.* **119** 3676–85
[54] Hernandez-Verdun D, Louvet E and Muro E 2013 Time-lapse, photoactivation, and photobleaching imaging of nucleolar assembly after mitosis *Methods Mol. Biol.* **1042** 337–50
[55] Konig I, Schwarz J P and Anderson K I 2008 Fluorescence lifetime imaging: association of cortical actin with a PIP3-rich membrane compartment *Eur. J. Cell Biol.* **87** 735–41
[56] Suhling K, Siegel J, Phillips D, French P M W, Leveque-Fort S, Webb S E D and Davis D M 2002 Imaging the environment of green fluorescent protein *Biophys. J.* **83** 3589–95
[57] Borst J W, Hink M A, van Hoek A and Visser A J W G 2005 Effects of refractive index and viscosity on fluorescence and anisotropy decays of enhanced cyan and yellow fluorescent proteins *Journal of Fluorescence* **15** 153–60
[58] Khorasanizadeh S 2004 The nucleosome: from genomic organization to genomic regulation *Cell* **116** 259–72
[59] Malik H S and Henikoff S 2003 Phylogenomics of the nucleosome *Nat. Struct. Biol.* **10** 882–91

[60] Luger K, Mader A W, Richmond R K, Sargent D F and Richmond T J 1997 Crystal structure of the nucleosome core particle at 2.8 A resolution *Nature* **389** 251–60
[61] Efron B 1979 Bootstrap methods: another look at the jackknife *Ann. Stat.* **7** 1–26
[62] Davison A C and Hinkley D V 1997 *Bootstrap Methods and Their Application* (Cambridge: Cambridge University Press)
[63] Lippincott-Schwartz J, Altan-Bonnet N and Patterson G H 2003 Photobleaching and photoactivation: following protein dynamics in living cells *Nat. Rev. Mol. Cell Biol.* **Supplement S** S7–S14
[64] Svoboda K and Yasuda R 2006 Principles of two-photon excitation microscopy and its applications to neuroscience *Neuron* **50** 823–39
[65] Misteli T 2008 Physiological importance of RNA and protein mobility in the cell nucleus *Histochemistry and Cell Biology* **129** 5–11
[66] Kimura H and Cook P R 2001 Kinetics of core histones in living human cells: little exchange of H3 and H4 and some rapid exchange of H2B *J. Cell Biol.* **153** 1341–53
[67] Musinova Y R, Lisitsyna O M, Golyshev S A, Tuzhikov A I, Polyakov V Y and Sheval E V 2011 Nucleolar localization/retention signal is responsible for transient accumulation of histone H2B in the nucleolus through electrostatic interactions *Biochimica Et Biophysica Acta-Molecular Cell Research* **1813** 27–38